11th World Congress on Computational Mechanics (WCCM XI)
5th European Conference on Computational Mechanics (ECCM V)
6th European Conference on Computational Fluid Dynamics (ECFD VI)
E. Oñate, J. Oliver and A. Huerta (Eds)

VERIFICATION OF POROUS LOSS MODEL FOR ASSESSMENT OF FLOW DIVERTERS

TAKASHI SUZUKI[*1], SYO KADOKURA[†1], HIROYUKI TAKAO[†2], SATOSHI TATESHIMA[†3], SHUNSUKE MASUDA[†2], DAHMANI CHIHEBEDDINE[†2,4], YI QIAN[†5], FERNANDO VINUELA[†3], YUICHI MURAYAMA[†2,3] AND MAKOTO YAMAMOTO[†6]

[*1] Graduate School of Mechanical Engineering
Tokyo University of Science
6-3-1 Niijyuku, Katsushika-ku, Tokyo, 125-8585, Japan
e-mail: j4512636@ed.tus.ac.jp

[†2] Department of Neurosurgery
Jikei University School of Medicine
3-25-8 Nishishinbashi, Minato-ku, Tokyo, 105-8461, Japan
e-mail: takao@jikei.ac.jp

[†3] Division of Interventional Neuroradiology
David Geffen School of Medicine at University of California Los Angeles
10833 Le Conte Avenue, Los Angeles, CA 90095, USA

[†4] Siemens Japan K.K.
Gate City Osaki West Tower, 11-1 Osaki 1-Chome, Shinagawa-ku, Tokyo, 141-8644, Japan

[†5] The Australian School of Advanced Medicine
Macquarie University
NSW 2109, Australia

[†6] Department of Mechanical Engineering
Tokyo University of Science
6-3-1 Niijyuku, Katsushika-ku, Tokyo, 125-8585, Japan
e-mail: yamamoto@rs.kagu.tus.ac.jp

Key Words: *Cerebral Aneurysm, Flow Diverter, CFD, Porous Loss Model.*

Abstract. Recently neurointerventional treatments using flow diverters (FDs) have been introduced and increasingly performed. However, complications (non-occluded and ruptured aneurysms after the treatment) have been reported. To assess the effects of FDs to the blood flow, Computational Fluid Dynamics (CFD) have been performed. In the approach using FDs geometries, higher machine specifications are required because of the larger number of computational elements due to the large scale difference between the size of the flow diverter's struts and the aneurysms. As an alternative method, we validate the applicability of

the porous model approach for patient-specific CFD. Two patients treated with FDs are analyzed. The results show that, in both cases, inflow rate into the aneurysms, velocity in the aneurysm and wall shear stress at the aneurysm surface are underestimated. However, pressure at the aneurysm surface are in good agreement between both models.

1 INTRODUCTION

Recently, flow diverters (below FDs) have been developed for the treatment of cerebral aneurysms. FDs are closed cell mesh cylinders comprised of many braided strands. Operators deploy these devices in the parent blood vessel to divert the blood flow away from the aneurysm itself. However non-occluded and ruptured cases after treatment indicate the existence of unresolved problems. To investigate the effects of FDs, Computational Fluid Dynamics (CFD) have been performed. Cebral et al. [1] analyzed 7 cases of aneurysms treated with FDs. They reported that the pressure in the treated aneurysm increased in each case ruptured after treatment. Larrabide et al. [2] also investigated hemodynamics variables for conditions before and after virtual FD implantation in 23 cases. The results showed that there was no significant changes in the intra-aneurysmal mean or peak pressure. In [1] and [2], Calculations were performed using FD geometries. To simulate the blood flow using FD geometries, it needs higher machine specifications because of the larger number of computational elements due to the large scale difference between the size of the flow diverter's struts and the aneurysms. For the alternative computational method, Augsburger et al. [3] proposed the modeling of FDs as a porous medium for one of FDs. They validated this model against the geometric approach and the porous medium approach in 2 patient-specific aneurysms. It has the possibility to predict the flow diversion effects for patients before treatment. However, the validation for large aneurysms and applying this approach for other FDs were not performed.

In this study, we validate the applicability of the porous model approach for different kinds of flow diverters. As a first step, we perform numerical simulations to determine the model coefficients. The model is based on Pipeline Embolization Device (PED; ev3/Covidien). After that, we compare the hemodynamics in the geometric and in the porous model approach. We validate that pressure at the aneurysm surfaces are in good agreement for both approaches.

2 METHODS

We performed patient-specific CFD simulations using 3D models obtained from digital subtraction angiography. Two patients (Fig. 1) treated with one of the Pipeline Embolization Device FDs were analyzed. The blood flow were simulated using ANSYS CFX 14.5 (ANSYS). In the flow field we assumed laminar flow since the Reynolds number based on the blood vessels diameter was around 500. The mass flow rate waveform[4] was imposed at the inlet boundary. At the outflow boundary, pressure was fixed to 0 Pa. Rigid and non-slip boundary conditions were assumed on all the vascular walls. The blood was assumed to be a Newtonian fluid with density and viscosity of 1,100 kg/m^3 and 0.0036 Pa·s respectively. The unsteady flow analysis were performed over two heartbeats (1.8 sec.) with a time step of 5×10^{-4} sec. The data of last one cycle were investigated in detail.

We compared two methods for reproducing the FD in the computations as shown in the

following subsections.

2.1 Geometric model approach

PED geometries fitted within the parent vessels were created using Amira (Visualization Sciences Group). And these geometries were imported as a stationary immersed solid in the simulations.

2.2 Directional loss model approach in a porous region

2.2.1 Directional loss model

We modeled PED as a porous region by the addition of a momentum source term to the Navier-Stokes equations. A streamwise-oriented coordinate system (x',y',z') such that the x' axis is aligned with the streamwise direction and y', z' axes lie on the transverse plane was used. In our computations, the streamwise direction (x') was defined as the normal vector to a cylinder surface replacing the PED geometries.

The directional loss model[3] is described as follows:

$$S_{M,x'} = -\frac{\mu}{K^S_{perm}} U_{x'} - K^S_{loss}\frac{\rho}{2}|\boldsymbol{U}|U_{x'} \tag{1}$$

$$S_{M,y'} = -\frac{\mu}{K^T_{perm}} U_{y'} - K^T_{loss}\frac{\rho}{2}|\boldsymbol{U}|U_{y'} \tag{2}$$

$$S_{M,z'} = -\frac{\mu}{K^T_{perm}} U_{z'} - K^T_{loss}\frac{\rho}{2}|\boldsymbol{U}|U_{z'} \tag{3}$$

where, μ and ρ are the viscosity and the density of blood respectively, $|\boldsymbol{U}|$ is the velocity magnitude, *Ux'*, *Uy'* and *Uz'* are the velocity components of the local coordinate system (x',y',z'). K^S_{perm}, K^T_{perm} are the streamwise and transverse permeabilities, and K^S_{loss}, K^T_{loss} are the streamwise and transverse loss coefficients. The linear components represent viscous losses and the quadratic terms represent inertial losses. Each coefficient was obtained via numerical simulations as described in the following subsections.

2.2.2 Determination of streamwise coefficients

A fully expanding PED was developed into a planar shape. Then, the PED was set perpendicularly to the flow. Fig. 2a shows the configuration. Boundary conditions were imposed as shown in Fig. 2b. The uniform flow velocity within the range of 0.1~1.0 m/s was imposed at the inlet boundary.

Figures 3 and 4 indicated the examples of the velocity field with the inflow velocity magnitude of 1.0 m/s at the X-Y plane dividing the computational domain and the graph of average pressure at the Y-Z plane respectively. A sudden pressure drop was observed through the FD region (x=0.0 mm), and after passing through the FD, the pressure increased gradually.

The relation between the pressure drop due to the porous model and Eqs. (1)~(3) is expressed as follows:

$$\Delta P = -S_{M,i'}\Delta e \tag{4}$$

where $i = x'$, y', z' and Δe is the thickness of the porous region. The pressure drop between the inlet and the outlet was obtained. Figure 5 showed the relation between the pressure drop and the imposed velocity magnitude. Applying a quadratic polynominal curve to the data in Fig. 5, $K^S_{perm}=1.9735\times10^{-10}$ m^2, $K^S_{loss}=2.9622\times10^{4}$ m^{-1} were obtained from combining Eqs. (1)~(4).

2.2.3 Determination of transverse coefficients

The same computational domain as section 2.2.1 was prepared. The inflow velocity profile within the range of 0.2~1.0 m/s at an angle with the streamwise direction was imposed as shown in Fig. 6. Next, the porous model was applied to the same computational domain instead of the PED geometry. Boundary conditions were imposed as shown in Fig. 6. The streamwise coefficients determined in the section 2.2.1 were used. Concerning the transverse losses, we assumed that viscous losses were dominant, therefore inertial losses were neglected. The average flow velocity angles at the outlet were compared between the computations using the geometric model and those using the porous model as shown in Fig. 7. To be accurate within less than 1% relative errors, the transverse permeability coefficients were adjusted.

In this research, the inflow velocity angle was fixed to 60 degrees. Figure 7 exhibits the example with the inflow velocity magnitude of 1.0 m/s. The obtained transverse permeability coefficients in each inflow conditions set were shown in Table 1. The average value of those results: $K^T_{perm}=2.5232\times10^{-10}$ m^2 was adopted.

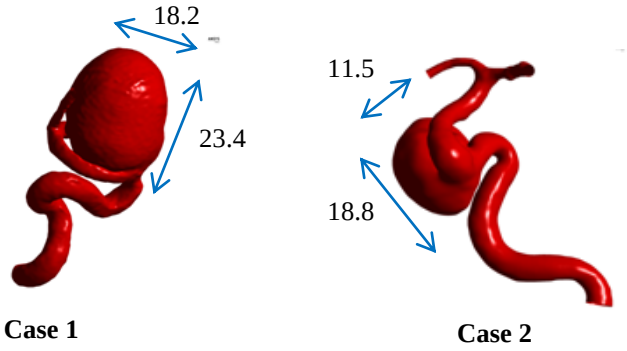

Figure 1: Computational targets

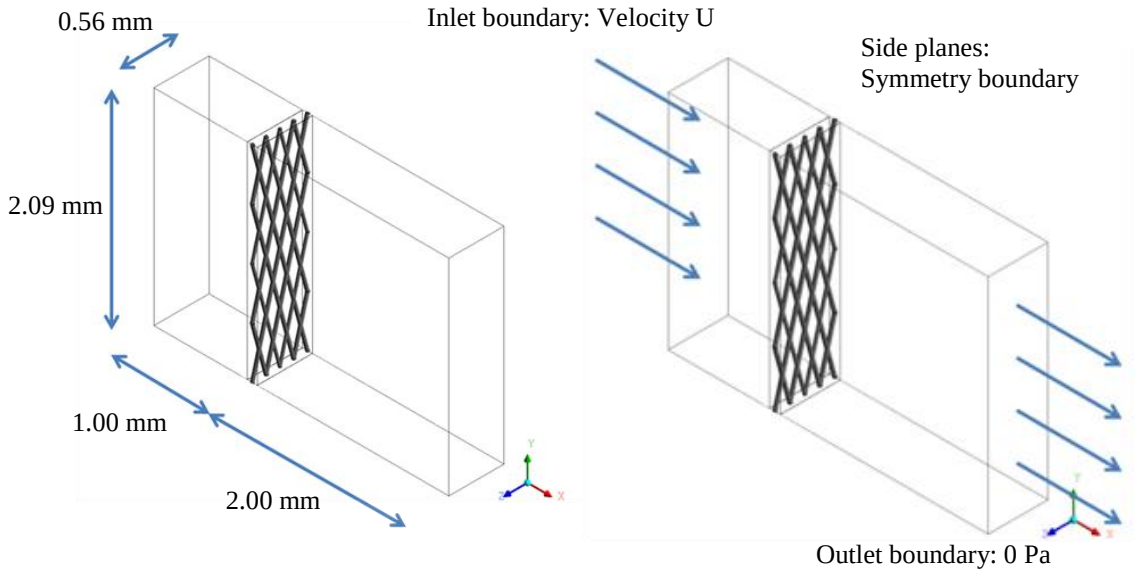

(a) Schematic diagram (b) Boundary conditions

Figure 2: Schematic diagram and boundary conditions of the computational domain (streamwise)

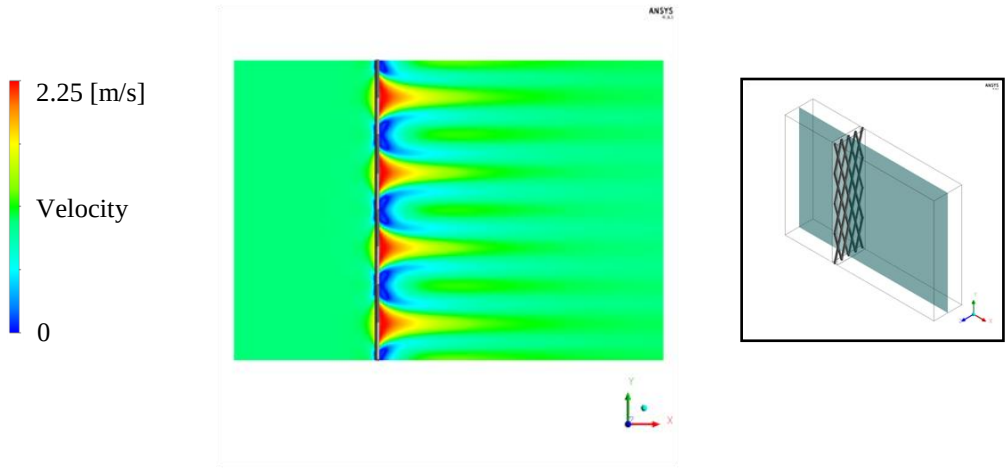

Figure 3: Example of the velocity field (Inflow velocity magnitude of 1.0 m/s)

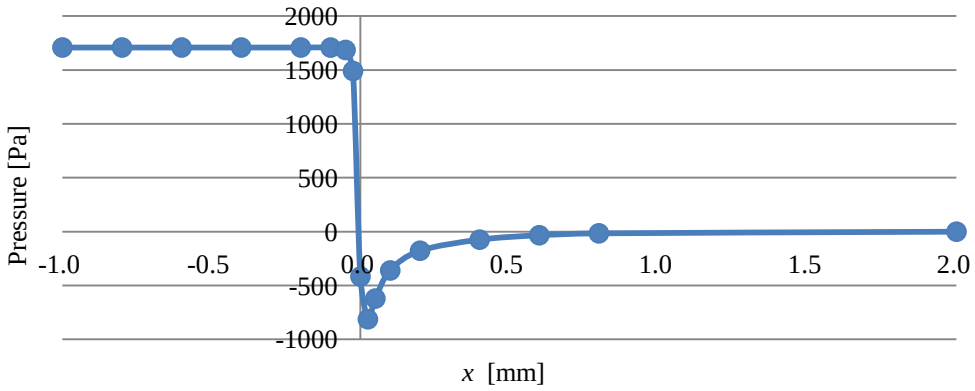

Figure 4: Average pressure at each Y-Z plane (Inflow velocity magnitude of 1.0 m/s)

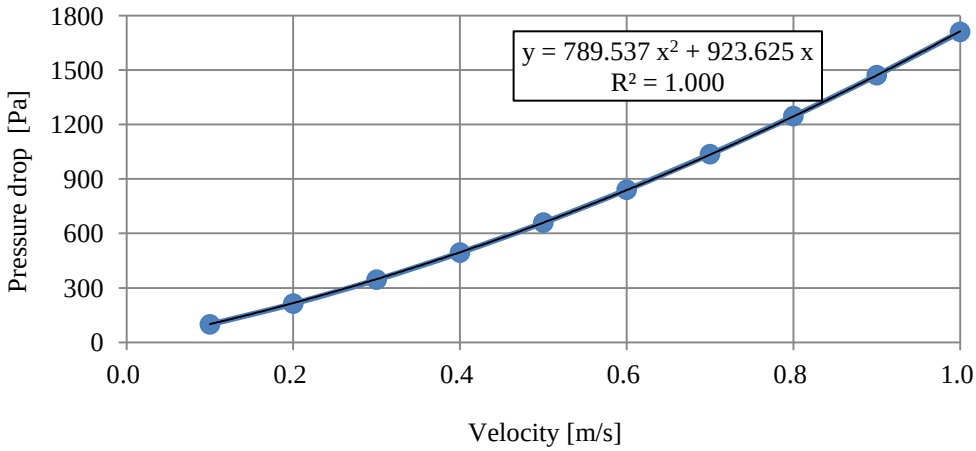

Figure 5: Pressure drop

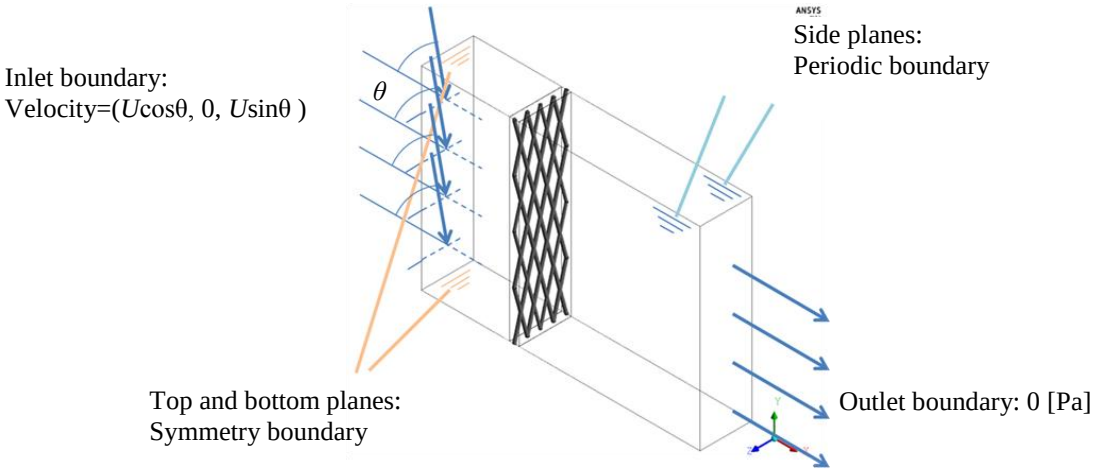

Figure 6: Boundary conditions of the computational domain (transverse)

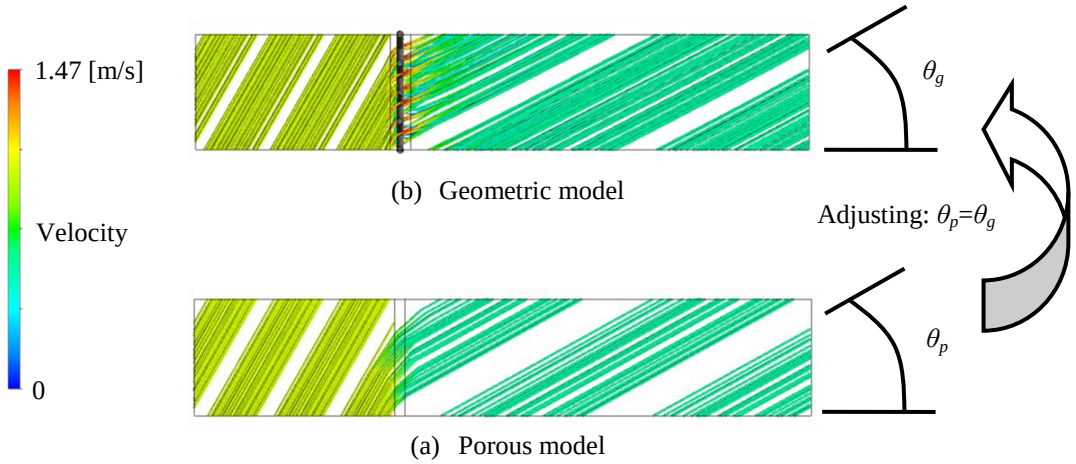

Figure 7: Example of adjusting outflow angle in the porous model approach to that in the geometric model approach (Velocity=1.0 m/s, Inflow angle=60 deg.)

Table 1: Transverse coefficients in each inflow condition

Inflow velocity [m/s]	K^T_{perm} ($\times 10^{-10}$) [m^2]	Area-average pressure at the inlet boundary (Geometric) [Pa]	Area-average pressure at the inlet boundary (Porous) [Pa]	Relative error [%]
0.2	2.4038	98.5	99.7	1.19
0.4	2.5723	212.3	219.1	3.08
0.6	2.6450	346.2	363.1	4.66
0.8	2.5535	500.4	533.4	6.18
1.0	2.4415	975.0	731.2	7.69
Average	**2.5232**			

3 RESULTS AND DISCUSSION

Figure 8 compares the streamline visualizations at the peak systole from two methods in case 1. It can be seen in both figures that the velocity in the aneurysm decreases because the flow becomes stagnant due to the large size of the aneurysm. Besides, the velocity in the aneurysm decreases additively by the reduction effects of the FD. In terms of the velocity magnitude, there is no clear qualitative difference. However, in the porous model approach, the jet flow into the aneurysm is dispersed before reaching the aneurysm wall. It confirms that the reduction effects of the FD is overestimated by the porous model approach.

Figure 9 shows the same comparison as Fig. 8 in case 2. It also can be seen in both figures that the velocity in the aneurysm decreases because of the same reasons as in case 1. In this case, no clear difference can be seen in the flow pattern in the aneurysm. However, from the view of streamline density, mass flow rate into the aneurysm is underestimated by the porous model approach.

Table 2 summarizes the values of the inflow rate into the aneurysm, the volume-average velocity in the aneurysm, area-average wall shear stress (*WSS*) and area-average pressure at the aneurysm surface. These values are the average of one cardiac cycle. The values of inflow

rate are normalized with the total mass flow rate. Table 2 indicates that the result in the porous model approach overestimates diversion effects quantitatively. In case 2, the relative error of inflow rate is 34.1%. This is twice larger than that in case 1. The largest error (48.8%) can be seen in the velocity magnitude in case 2. In both cases, the absolute values are very low, and it could be a main cause of the large relative errors. Large relative errors also can be seen in the WSS parameter. These are presented by the large relative errors in the velocity magnitude. However, the relative errors about the pressure are less than 5%, and it shows good agreement.

Figure 10 shows the cross-sections of the aneurysmal neck. The Color map represents the mass flow rate through the neck at peak systole. Mass flow rate of inflow into the aneurysms takes positive values. On the other hand, that of outflow from the aneurysms takes negative value. Red arrows point the direction of flow. From these figures, we can see that the outside corners of the FD are stretched, and the wire density of the FD becomes small at these locations. In these locations, mass flow rate takes high positive value. That is, much inflow into the aneurysm goes through the locations of the FD in which wire density is small locally. In the porous model approach, this locally small wire density is not taken into account. It could cause the overestimation of reduction effects in the porous model approach.

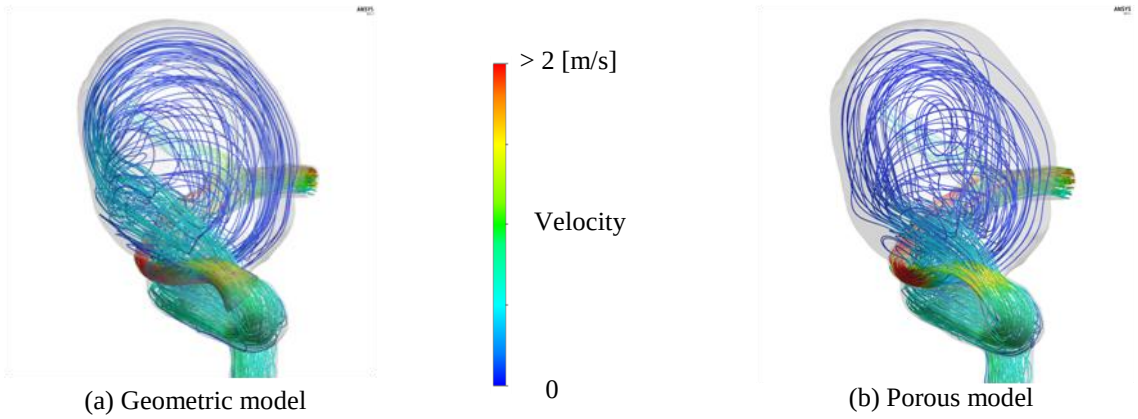

(a) Geometric model (b) Porous model

Figure 8: Comparison of streamline visualization between Geometric and Porous model (Case 1)

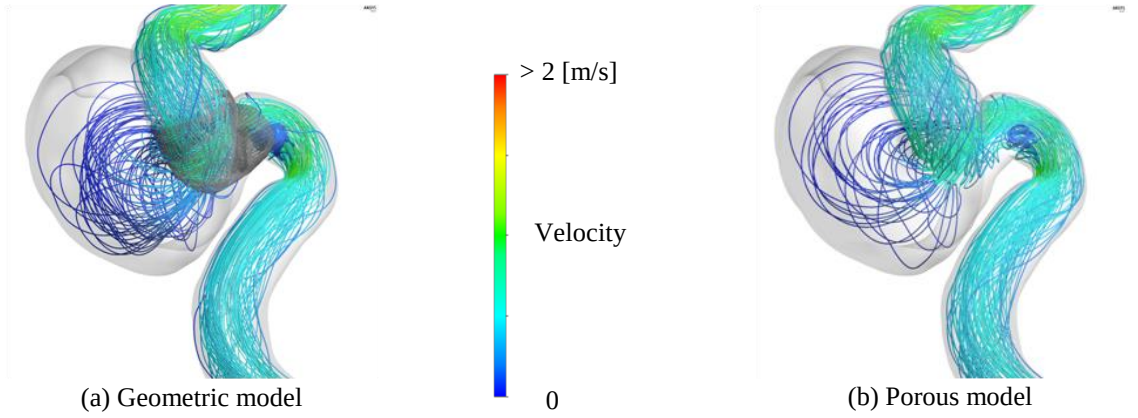

(a) Geometric model (b) Porous model

Figure 9: Comparison of streamline visualization between Geometric and Porous model (Case 2)

Table 2: Comparison of parameters

		Geometric model	Porous model	Time average relative error [%]
Inflow into the aneurysm	Case 1	0.737	0.611	17.2
	Case 2	0.383	0.254	34.1
Volume-average velocity in the aneurysm [m/s]	Case 1	0.0659	0.0439	32.2
	Case 2	0.0283	0.0145	48.8
Area-average wall shear stress at the aneurysm surface [Pa]	Case 1	0.768	0.459	39.1
	Case 2	0.285	0.154	46.2
Area-average pressure at the aneurysm surface [Pa]	Case 1	3091	3216	4.1
	Case 2	3118	3136	0.6

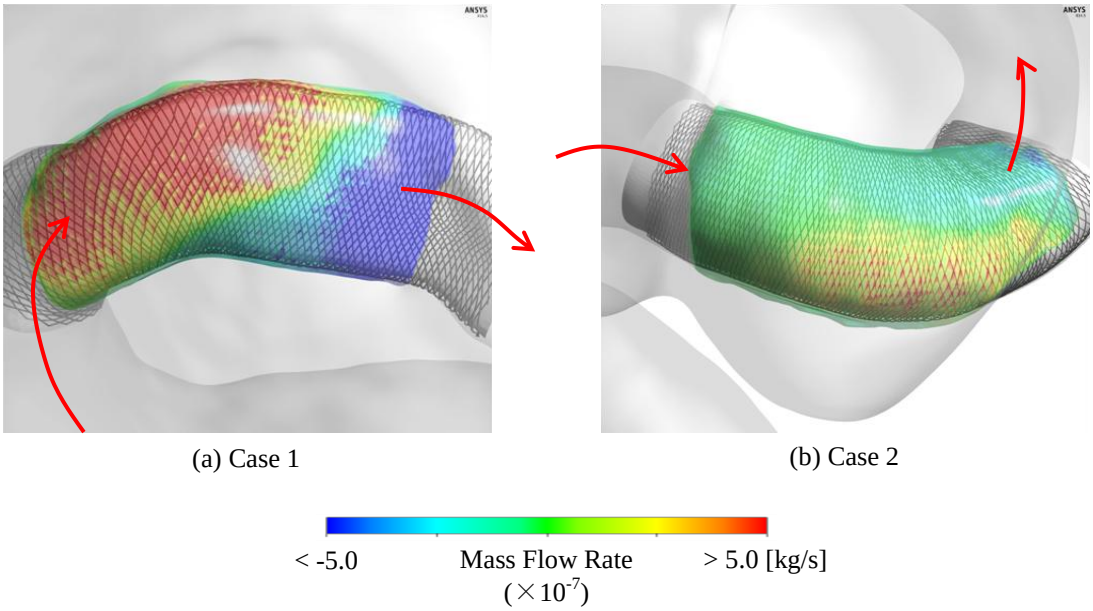

Figure 10: Mass flow rate at the neck closs-sections

4 CONCLUSIONS

To apply the porous model approach for one of the PED flow diverters, we validated the applicability of this approach by comparing hemodynamic parameters between this approach and the geometric approach. We performed patient-specific CFD for 2 cases. The results from this investigation are summarized as follows:

- By comparing both approaches, similarity in the flow patterns in the aneurysm was identified.
- With the porous model approach, inflow rate into the aneurysm, velocity in the aneurysm and wall shear stress at aneurysm surface are underestimated.
- Pressure values at the aneurysm surface are in good agreement between the porous

and the geometric model approach.

- In order to refine the porous model approach, it would be needed to consider the local porosity differences of the FD due to the deformation along with the artery curve.

REFERENCES

[1] Cebral, J. R., Mut, F., Raschi, M., Scrivano, E., Ceratto, R., Lylyk, P. and Putman, C. M. Aneurysm Rupture Following Treatment with Flow-diverting Stents: Computational Hemodynamics Analysis of Treatment. *AJNR Am J Neuroradiol.* (2011) **32**:27-33.

[2] Larrabide, I., Aquilar, M. L., Morales, H. G., Geers, A. J., Kulcsár, Z., Rüfenacht, D. and Frangi, A.F. Intra-aneurysmal Pressure and Flow Changes Induced by Flow Diverters: Relation to Aneurysm Size and Shape. *AJNR Am J Neuroradiol.* (2013)**34**:816-822.

[3] Augsburger, L., Reymond, P., Rufenacht, D. A. and Stergiopulos, N. Intracranial Stents Being Modeled as a Porous Medium: Flow Simulation in Stented Cerebral Aneurysms. *Ann Biomed Eng*. (2010) **39**(2):850–863.

[4] M. D. Ford, N. Alperin, S. H. Lee, D. W. Holdsworth, and D. A. Steinman Characterization of volumetric flow rate waveforms in the normal internal carotid and vertebral arteries. *Physiol. Meas.* (2005) **26**:477-488.